

Breakup of carbon nanotube flocs in microfluidic traps

Paul R. Start, Steven D. Hudson*, Erik K. Hobbie, Kalman B. Migler

Polymers Division, National Institute of Standards and Technology, Gaithersburg, MD 20899-8542, USA

Received 21 August 2005; accepted 20 November 2005

Available online 20 December 2005

Abstract

The critical stress to break flocs of multiwalled-carbon nanotubes suspended in low-molecular-weight polymer fluid is measured in planar elongational flow. Through image analysis of aggregates and their fragments, the extension rate of the flow and the size and aspect ratio of the aggregates are measured in real time. While trapping an aggregate at the stagnation point of the device, the flow rate is increased continually and breaking events are recorded, establishing a correlation between aggregate size and the critical elongation stress for fragmentation σ . This relationship resembles that for the breakup of flocs comprising spherical particles, yet it indicates that the strength of these fibrous flocs depends much more strongly on the local particle concentration. Fracture avalanches (or cascades) are also observed.

Published by Elsevier Inc.

Keywords: Dispersion; Breakup; Nanotubes; Flocs; Microfluidics; Elongational flow

1. Introduction

Particle suspensions are ubiquitous in both nature and industry, and operations designed to disperse particles in fluids are critical to a number of industrial processes involving soft materials. Knowledge of the kinetics of particle dispersion and its ultimate limits are therefore crucial for efficient processing. For fractal aggregates comprising spherical particles, Sonntag and Russel [1–3] have measured the critical stress for cluster breakup, which they relate to the fractal geometry of the cluster through a simple power-law involving aggregation number and stress. More recently, the hydrodynamic dispersion of spherical calcium carbonate agglomerates was studied under both steady and oscillatory shear-flow conditions [4]. For a given steady shear stress, erosion rates were found to be strongly influenced by the cohesive strength of the agglomerates with less cohesive, low-density clusters exhibiting faster erosion than high-density clusters [4]. The dispersion kinetics were also found to be influenced by the extent of matrix infiltration within the agglomerate, with more infiltration resulting in reduced erosion rates [4].

The formation and breakup of clusters and aggregates in flowing fiber suspensions has also received recent attention, both through numerical simulations [5] and—in the case of carbon nanotubes—rheo-optical measurements [6] of flow-induced aggregation at low stress and flow-induced dispersion at high stress. Here, we examine the breakup of clusters composed of multi-walled carbon nanotubes suspended in low-molecular-weight polyisobutylene under extensional flow fields produced in a cross-channel microfluidic device. Flow enters through opposing channels and exits orthogonally through the other two channels, creating an extensional flow field with a stagnant zone in the region where the channels intersect. Although a particle or floc positioned precisely at the stagnation point may remain trapped there indefinitely, in practice the exit flow rates must be tuned continuously to maintain trapping. Similar microfluidic traps have been used to investigate the stretching of macromolecules in flow [7]. In some traps, the type, as well as the rate, of flow is adjustable, mimicking the behavior of a four-roll mill [8]. By analyzing images of clusters and their fragments, the extensional rate of the flow and the size and aspect ratio of the aggregates are measured in real time. While trapping an aggregate at the stagnation point of the device, the flow rate is continually increased and breaking events are recorded, establishing a correlation between cluster

* Corresponding author. Fax: +1 301 975 4924.

E-mail address: steven.hudson@nist.gov (S.D. Hudson).

size and stress. We compare these measurements with clustering and breakup data in simple shear.

2. Experimental

A modified cross-channel device (Fig. 1) was created following a method for microfluidic construction described by Harrison, Cabral and others [9,10]. A UV-curable thiolene-based optical adhesive (#61, Norland Products [11]) was patterned onto a glass slide using a transparency mask. Curing was performed using a Spectroline SB-100P flood lamp optimized for 365 nm wavelength illumination. The desired feature height is obtained through control of total exposure [10]. The resulting product serves as a master for replication and molding of the actual device. Polydimethylsiloxane (Sylgard 184, Dow Corning) and a thermal curing agent were mixed at 10:1 mass ratio and poured over the patterned substrate. The PDMS was allowed to de-gas under vacuum for about 1 h, followed by curing at 75 °C for at least 1 h. The transparent, solid, flexible, cross-linked PDMS was then peeled from the patterned substrate, exposing the microfluidic channels. Using an 18-gauge blunt tipped needle, holes were bored through the PDMS for connection of the channels to tubing and syringe pumps. The PDMS device was then bonded to a glass slide. The slide was first exposed to UV light using a Jelight 342 UVO cleaner for approximately 30 min. Without removing the glass slide, the face of the device to be bonded to the glass was exposed to the UV source for approximately 1 min. The UV exposed surfaces were then brought into contact and placed in an oven at 75 °C overnight. Tubing with metal fittings was connected to the previously bored holes and held in place with fast curing epoxy. The finished device can then be filled with the materials of interest and connected to syringe pumps.

One channel is for sample input and another is for balancing the flow rate through the exit channels (Fig. 1). Adjustment of the flow rate through this latter channel allows one to compensate for any drift of a cluster positioned at the center of the cross channels. However, to minimize drift, a fast response time is needed at the center of the cross channel when a change in the flow rate is made through the balance channel. The response time of the device is proportional to the resistance of liquid flowing through the channels, and hence the viscosity

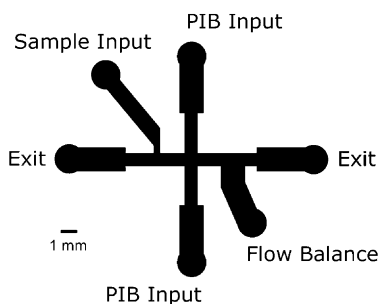


Fig. 1. Scale drawing of the cross-channel microfluidic device. The nanotube suspension is injected from the sample input. Horizontal positioning of aggregates is accomplished by injecting or withdrawing from the flow balance port. Planar extensional flow is established at the cross-channel center by pumping fluid into the PIB input channels.

of the liquid and the device dimensions. Optimization of the device dimensions is important to achieve the desired performance. Channel lengths were kept to a minimum, with the total length of the input channels, from one input to the other, being approximately 1.2 cm. Channel width and depth near the center of the cross channels was approximately 800 μm . Away from the central cross-channel region, channel widths were increased to reduce resistance to flow.

Multi-walled carbon nanotubes (MWNTs) were grown via chemical vapor deposition. From electron microscopy, the mean diameter is $a \approx 50$ nm (polydispersity ≈ 1.5). Due to their length and optical contrast, individual MWNTs are discernible in optical micrographs of $25\times$ or higher, and from $200\times$ images of thin-film dispersions, the mean length is $\ell \approx 12$ μm (polydispersity ≈ 2.0). The suspending fluid used here is polyisobutylene (PIB from PolySciences, nominal molar mass 500) with a shear viscosity of 0.5 Pa s at 25 °C. Dispersions are prepared by dissolving the PIB in sonicated MWNT-toluene suspensions, which are stirred continuously as the solvent is removed. The suspensions contain a succinimide polymer (1:1 MWNT by mass, PIB soluble) as a dispersant [6], but the final PIB suspensions used here are only marginally stable, with weak flocculation occurring over the course of hours to days. Strong to modest shearing is sufficient to redisperse the tubes, however, consistent with a weak reversible attraction, and hydrodynamic forces dominate over thermal forces in the non-Brownian PIB suspensions. Suspensions of primary interest here contain 10^{-2} mass-fraction MWNT in PIB and are semi-dilute to concentrated, with $n\ell^3 \approx (4/\pi)\phi_0(\ell/a)^2 \approx 250$ and $n\ell^2a \approx (4/\pi)\phi_0(\ell/a) \approx 1$, where n is the number of tubes per unit volume and $\phi_0 \approx 3.4 \times 10^{-3}$ is the volume fraction. Weak shear flow promotes aggregation in this type of non-Brownian nanotube suspension. Although the nanotubes in PIB are only very slowly sedimenting, large clusters sediment over the course of hours. The syringe connected to the sample input channel is filled with the MWNT-PIB suspension, while the device itself and all other syringes are filled with pure PIB.

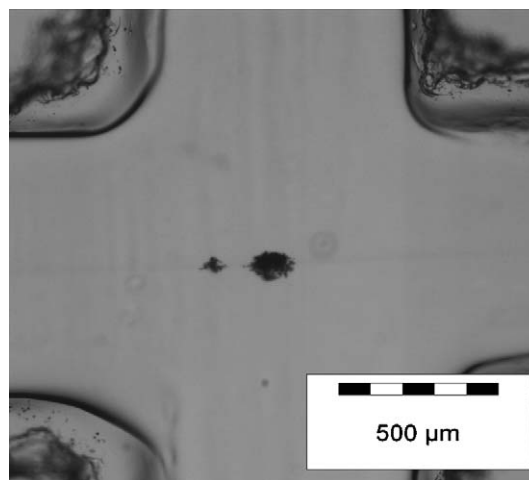


Fig. 2. Image of a nanotubes aggregate (approximately 80×125 μm) and its fragment (approximately 45×65 μm) separating toward the left. The channel width is approximately 800 μm . The scale bar is dashed, so that each sub-unit is 100 μm in length.

Imaging of the MWNT flocs within the microfluidic device was carried out (e.g., Fig. 2) on an Olympus [11] IX71 inverted optical microscope equipped with a CCD camera for image capture. Objective lenses with magnification ranging from 4× to 40× were used to view the clusters in the flow fields, but for most experiments a 10× objective (NA = 0.30) was used. Image magnification was determined using a calibrated ruling. Image analysis, control of the syringe pumps, and data processing were all done in real time using routines written in LabVIEW 7.0. Gray-scale images of the central cross-channel region are acquired. Appropriate thresholding of the images identifies any present clusters. Floc size is measured in number of pixels and the flocs are ranked according to size. The largest is deemed the parent cluster. Floc position is determined by the “center of mass” of the two-dimensional projected image. Over the course of multiple frames a trajectory for each floc is recorded. Additionally, the length of the perimeter, the aspect ratio, and the orientation for all clusters are recorded for each frame.

To observe a cluster over long times it is necessary to trap it at the stagnation point of the converging input flows. No control routines are required to keep the cluster centered vertically between the converging input flows. Their opposing and balanced flow keeps the cluster centered. The cluster will, however, drift to the left or right toward either exit channel. Trapping of the parent cluster at the stagnation point is achieved by adjusting the flow rate through the flow balance channel. The magnitude and direction of these adjustments are determined based upon the parent cluster’s velocity and position relative to the center of the field of view. These adjustments are handled in real time through the PID controlled feedback loop. As a parent cluster near the stagnation point begins to drift, an adjustment in the flow rate and flow direction through the flow balance channel compensates and brings the cluster back to the center. With proper adjustment of the appropriate parameters we were able to trap MWNT clusters at the stagnation point under a range of input flow rates with minimal drift over extended

times. This system allows one to observe phenomena such as cluster deformation and breakup as a function of time and extension rate.

The following protocol was developed to examine the breakup of MWNT flocs under the extensional flow conditions.

1. Inject a mass of MWNTs through the sample input channel and draw them into the central cross-channel region.
2. Set flow rate through input channels to 0.01 ml/h. At this low flow rate excess MWNT material is slowly swept out of the field of view. Within a minute individual MWNT clusters are observed.
3. Isolate a single MWNT cluster near the stagnation point. Adjustments are made to focus, microscope illumination, and threshold settings to properly image the isolated floc. Enabling the PID feedback control traps the cluster at the stagnation point and allows for continued observation over time.
4. Increase the input flow rates in small steps over time (Fig. 3). As the extension rate increases the forces on the cluster increase. At some point the extension rate is just large enough to cause breakup. This is the critical extension rate for breakup.
5. Calculate the extension rate at breakup based upon relative positions of the fragment and main cluster over sequential frames.
6. Allow the cluster to stabilize and then continue to increase input flow rates, examining further fragmentation events.

This allows one to determine the critical extension rate for breakup of a given cluster. When increasing the input flow rates, small step sizes relative to the current input flow rates are necessary. Large step sizes will cause fragmentation, but will not allow one to study the minimum forces required to cause breakup. As breakup occurs the software routines automatically select the largest fragment and keep it trapped at the stagnation point. The cluster that remains will have different characteris-

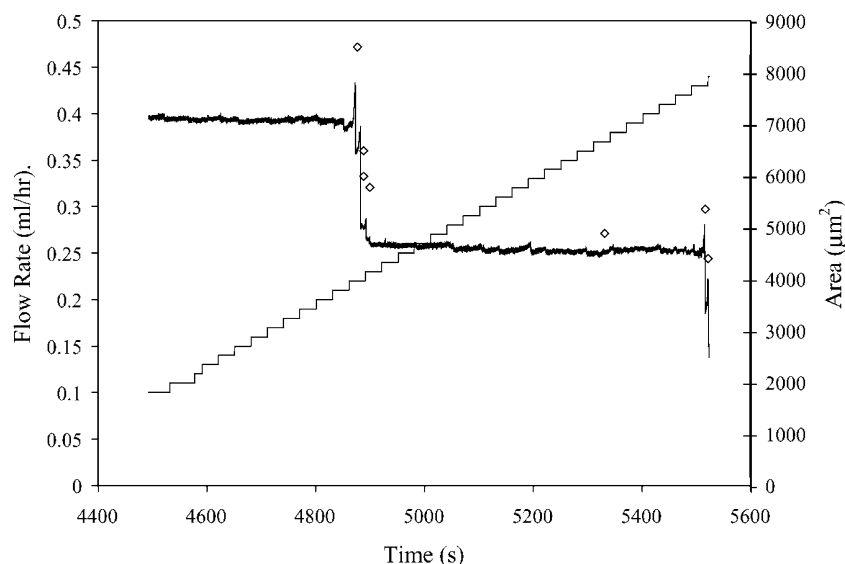


Fig. 3. An experimental trace of parent floc size as a function of flow rate, which was increased with time, as indicated. Fracture events are noted with symbols.

tics. It will be smaller, and its shape, including perimeter and aspect ratio, will be different than the original floc. Frequently there are additional fragments that break free. The ejection of these secondary fragments is likely related to instability of the floc after the first fragment is removed. Therefore, a cluster is allowed to reach stability as other fragments are ejected before continuing to increase the input flow rates.

In addition to a difference in density between the MWNT floc and the surrounding PIB fluid, there is a velocity gradient in the vertical direction of the device, and at a given input flow rate the extension rate near the floor or the ceiling will be lower than at intermediate heights. Over time the floc will thus migrate to the floor of the microfluidic channel, and as it does so the flow fields surrounding it will change. Because of this, long-term experiments at constant flow rates cannot be performed. For the procedure described above, the experiment typically ends when the cluster has migrated to the bottom of the channel, a process that typically takes about 30 min. The cluster is then allowed to exit and the procedure of isolating and testing another floc is repeated.

3. Results

The data recorded over the course of the experiment include the position, area, perimeter, aspect ratio, and orientation for the parent cluster and all other flocs within the field of view. These other flocs include an occasional cluster that enters with the input flow, and more importantly, any fragments that are ejected from the parent cluster. Data are recorded over time, typically at intervals of 0.2 s. Extension rates for ejected fragments are calculated for each sequential captured frame using

$$\dot{\epsilon} = \frac{(x_i - x_{i-1})}{(t_i - t_{i-1})x_{i-1}}, \quad (1)$$

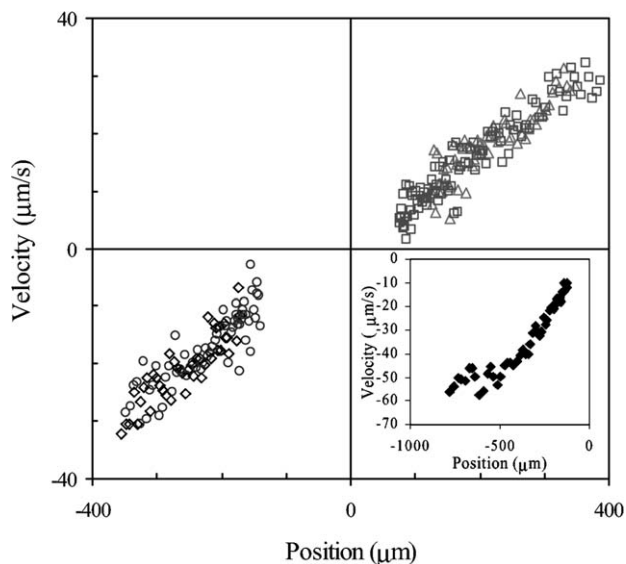


Fig. 4. Velocity vs position for a series of four fragments under identical flow conditions. Input flow rate = 0.07 ml/h. Calculated extension rates: 0.083 ± 0.011 , 0.085 ± 0.008 , 0.082 ± 0.010 , and $0.083 \pm 0.009 \text{ s}^{-1}$. Inset is the velocity of another fragment, showing saturation of the velocity as the fragment proceeds further from the stagnation point and enters into the exit channel.

where t is the time associated with a particular frame and x is the center of mass position of the ejected fragment at time t . At early times as a fragment is breaking free of the parent cluster, the calculated extension rates are influenced by remaining ties to the parent cluster or the distorted flow fields around it. Additionally, at later times, as the ejected fragment enters the exit channels the calculated extension rate will be influenced by the channel walls. Therefore, extension rates are averaged only over the intermediate frames.

Fig. 4 (inset) shows a plot of velocity as a function of position for a fragment ejected from the parent cluster and accelerated to the left. The zero position corresponds to the center of the cross-channel device. The break in the slope of the velocity profile corresponds to the fragment entering the exit channel where it experiences a different flow field. Fig. 4 shows the velocity vs position for a series of four fragments ejected from a parent cluster under identical flow conditions. Averaged extension rate values are in good agreement with each other. The linearity of this plot demonstrates the uniform nature of the extensional flow field. Moreover, as long as the cluster has not settled significantly, the extension rate indicated by the ejected fragments is proportional to the volumetric flow rate.

A wide range of fragment sizes is generated, with the majority being relatively small in comparison to the parent cluster (Fig. 5). There is no correlation of relative fragment size with parent size (see inset), extension rate, stress, aspect ratio, or time interval between fractures. As shown in Fig. 3, some fracture events are isolated and others occur in rapid succession, as in an avalanche. The distribution of time interval between fractures is uniform, and there is no correlation between relative fragment size and time interval. Having determined the extension rate for each breaking event, we now seek the associated fracture stress, σ . The hydrodynamic stress on the cluster is of course proportional to the extensional rate and the viscosity of the surrounding fluid. The stress is also roughly proportional to the aspect ratio of the cluster L/d , and therefore we set

$$\sigma = 3\eta\dot{\epsilon}L/d. \quad (2)$$

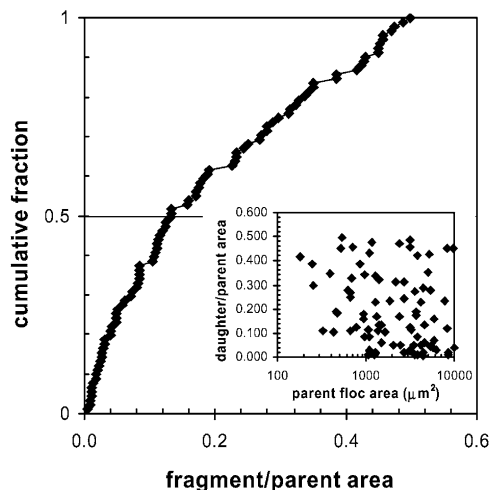


Fig. 5. Cumulative fraction of fragments versus size relative to the parent cluster. Inset: relative fragment size vs parent cluster size.

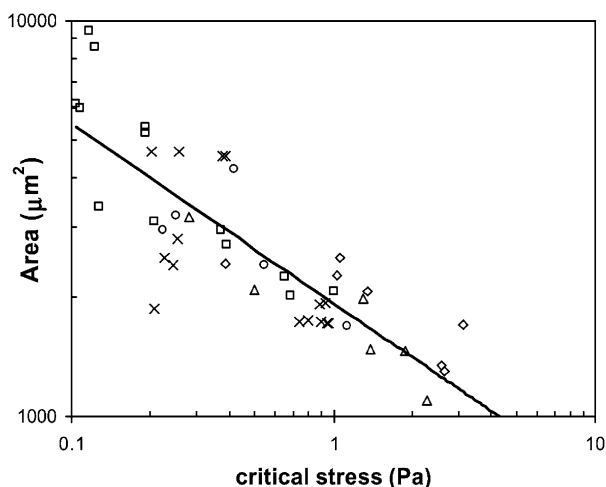


Fig. 6. Cluster area plotted vs fragmentation stress (Eq. (2)) for several flocs, exhibiting a power-law relation $A \sim \sigma^{-0.45 \pm 0.04}$.

In reality, the hydrodynamic drag force is more complicated, since the flow field in and around the cluster depends on additional details of its geometry [12,13].

For large floc area, a power-law inverse relationship between stress σ and floc area is observed, as expected (Fig. 6). However, for sufficiently small flocs (approximately 50 μm or less), the power-law relationship breaks down, after a final fracture avalanche. The surviving small fragment (roughly 10–30 μm in size, comparable to the longest fibers) is generally much more robust and withstands substantially higher stress. In the first regime, described by a power-law relationship, A scales as $\sigma^{-0.45 \pm 0.04}$, a substantially weaker function of stress than that for spherical particle flocs, where A proportional to $\sigma^{-0.71}$ was found [1].

4. Discussion

The mass fraction of nanotubes in the sample input is 0.01. The concentration within a cluster is expected to be nearly this nominal value; however, slight variations are expected. In particular, concentration variations within the clusters are expected to be fractal, with a two-point density correlation function that spatially decays with a fractional power law as r^{D_f-3} in three dimensions, where D_f is the fractal dimension of the floc. The fractal dimension depends on the type of aggregation [14,15], the aspect ratio of the constituents [16], and flow if the aggregate deforms [12]. Based on these factors, a fractal dimension of around 2.2–2.6 might be expected here, with data specific to identical nonBrownian carbon nanotube suspensions suggesting $D_f \approx 2.5$ [17]. The fractal geometry of the clusters is important because each the elastic modulus and yield strength of the cluster is a strong function of the concentration, typically showing power law behavior with an exponent [18]

$$\alpha = (3 + D_b)/(3 - D_f) \quad (3)$$

in three dimensions, where D_b is the backbone dimension of the network, which in this case is unity [17]. Aggregates of spherical particles are characterized by an exponent α of approximately 4 [1,17]. Rheological experiments on these MWNT

suspensions suggest that α is somewhat larger, being approximately 7, which is a direct consequence (consistent with Eq. (3)) of the relatively large fractal dimension for diffusion-limited cluster aggregation in large-aspect-ratio rigid rods [16,17]. Slight variations in concentration thus have an even more significant effect on the strength and breakup of these aggregates.

The mass of a fractal aggregate is proportional to R^{D_f} , where R is the radius, or equivalently to $A^{D_f/2}$. Therefore, assuming $D_f = 2.5$, the data in Fig. 6 suggest that the mass of a cluster is proportional to $\sigma^{-0.57 \pm 0.08}$. Taking Eq. (3) together with theoretical analysis by Sonntag and Russel this exponent is predicted to be $[1,18] -D_f/(3 + D_b) = -0.63$, with which the data is in close agreement. Each of these values for this exponent is significantly less than that measured for spherically symmetric aggregates of spherical particles in simple shear flow [3], viz. approximately -0.88 . A variety of factors may be responsible for this apparent difference. Most notably, the larger exponent α observed for these nonBrownian nanotube systems is expected to reduce the magnitude of the critical stress mass exponent [1]. The type of flow may also be an offsetting factor: Higashitani et al. suggest that the exponent is of larger magnitude in extensional flow [12].

5. Summary

The critical stress to break aggregates of multiwalled-carbon nanotubes suspended in low-molecular-weight polymer fluids has been measured in planar elongational flow produced in a microfluidic device. Through an image analysis of aggregates and their fragments, the extension rate of the flow and the size and aspect ratio of the aggregates have been measured in real time. While trapping an aggregate at the stagnation point of the device, the flow rate was continually increased and breaking events (which included cascades) were recorded, establishing a correlation between floc size and stress. That the floc size depends rather weakly on stress indicates that the floc strength depends very strongly on local particle density.

Acknowledgment

Support from the NIST Materials Science Engineering Laboratory Director's Reserve is greatly appreciated.

References

- [1] R.C. Sonntag, W.B. Russel, J. Colloid Interface Sci. 115 (1987) 378.
- [2] R.C. Sonntag, W.B. Russel, J. Colloid Interface Sci. 115 (1987) 390.
- [3] R.C. Sonntag, W.B. Russel, J. Colloid Interface Sci. 113 (1986) 399.
- [4] P. Levresse, I. Manas-Zloczower, D.L. Fekke, Rubber Chem. Technol. 75 (2002) 119.
- [5] L.H. Switzer, D.J. Klingenberg, Nordic Pulp Paper Res. J. 18 (2003) 141.
- [6] S. Lin-Gibson, J.A. Pathak, E.A. Grulke, H. Wang, E.K. Hobbie, Phys. Rev. Lett. 92 (2004) 048302.
- [7] C.M. Schroeder, H.P. Babcock, E.S.G. Shaqfeh, S. Chu, Science 301 (2003) 1515.
- [8] S.D. Hudson, et al., Appl. Phys. Lett. 85 (2004) 335.
- [9] C. Harrison, J. Cabral, C.M. Stafford, A. Karim, E.J. Amis, J. Micromech. Microeng. 14 (2004) 153.

- [10] J.T. Cabral, S.D. Hudson, C. Harrison, J.F. Douglas, *Langmuir* 20 (2004) 10,020.
- [11] Certain commercial materials and equipment are identified in this paper in order to adequately specify the experimental procedure. In no case does such identification imply recommendation or endorsement by the National Institute of Standards and Technology, nor does it imply that these are necessarily the best available for the purpose.
- [12] K. Higashitani, K. Imura, H. Sanda, *Chem. Eng. Sci.* 56 (2001) 2927.
- [13] S. Blaser, *Chem. Eng. Sci.* 57 (2002) 515.
- [14] M. Kolb, R. Jullien, *J. Phys. Lett.* 45 (1984) L977.
- [15] D.A. Weitz, J.S. Huang, M.Y. Lin, J. Sung, *Phys. Rev. Lett.* 54 (1985) 1416.
- [16] A. Mohraz, D.B. Moler, R.M. Ziff, M.J. Solomon, *Phys. Rev. Lett.* 92 (2004) 155,503.
- [17] E.K. Hobbie, submitted for publication.
- [18] W.H. Shih, W.Y. Shih, S.I. Kim, J. Liu, I.A. Aksay, *Phys. Rev. A* 42 (1990) 4772.